

# Angular response of a triangular optical cavity analyzed by a linear approximation method

SATOSHI TANIOKA<sup>1,2,\*</sup>, GUI-GUO GE<sup>3</sup>, KEIKO KOKEYAMA<sup>4</sup>, MASAYUKI NAKANO<sup>5</sup>, JUNEGYU PARK<sup>6</sup>, AND KIWAMU IZUMI<sup>7</sup>

<sup>1</sup>The Graduate University for Advanced Studies (SOKENDAI), Mitaka, Tokyo 181-8588, Japan

<sup>2</sup>National Astronomical Observatory of Japan (NAOJ), Mitaka, Tokyo 181-8588, Japan

<sup>3</sup>State Key Laboratory of Magnetic Resonance and Atomic and Molecular Physics, Wuhan Institute of Physics and Mathematics, Chinese Academy of Sciences, West No. 30, Xiaohongshan, Wuhan, 430071, China

<sup>4</sup>Institute for Cosmic Ray Research (ICRR), The University of Tokyo, Higashi-Mozumi 238, Kamioka-cho, Hida-shi, Gifu 506-1205 Japan

<sup>5</sup>Department of Physics, University of Toyama, Toyama City, Toyama 930-8555, Japan

<sup>6</sup>Department of Physics, Sogang University, One Sinsu-Dong, Mapo-Gu, Seoul, 121-742, Korea

<sup>7</sup>Institute of Space and Astronautical Science, 3-1-1 Yoshinodai, Chuo ward, Sagami-hara, Kanagawa 252-5210, Japan

\*Corresponding author: satoshi.tanioka@nao.ac.jp

Compiled February 11, 2021

---

A triangular optical cavity is often used as a mode cleaning cavity in precision laser interferometry such as gravitational wave detectors. An alignment sensing and control system for maintaining the alignment of a mode cleaning cavity with respect to the incoming laser beam is critical for detector's performance. Therefore, understanding the behavior of the angular response is vital to both design and commissioning test of the alignment control system. We present a linear approximation approach which not only simplifies the computation but also provides a comprehensive picture of the angular response. The observable degrees of freedom in a triangular cavity is discussed based on the linear approximation. © 2021 Optical Society of America

<http://dx.doi.org/10.1364/ao.XX.XXXXXX>

---

## 1. INTRODUCTION

Optical cavities are widely used in precision measurement, such as gravitational wave detection [1] and optical lattice clock [2]. In gravitational wave detectors, one or more triangular cavities, called the input mode cleaners (IMCs), are employed. The IMCs provide three critical functionalities — spatial mode cleaning, polarization selection and frequency stabilization [3, 4].

The IMC is often an isosceles triangular cavity with the length of one side much shorter than the other two due to spatial constraint given by the vacuum envelope while maintaining tens of meters or more in the optical round trip length. It is often the case that the triangular cavity is usually preferred because it does not require an additional optical isolator to extract the field in reflection such that its phase information is used to keep the cavity resonant. The apex mirror is a curved mirror while the other two are flat mirrors as shown in Fig. 1.

Each mirror in the IMC is suspended to reduce seismic motions which, in turn, lead to angular drifts. Angular drifts directly introduce misalignment in the cavity axis. Such a misalignment can deteriorate detector sensitivity and stability by increasing a few noise couplings including those to length

fluctuation and beam jitter. Moreover, angular misalignment causes light in the fundamental mode to be coupled into higher-order spatial modes, reducing the amount of power injected to the main part of gravitational wave detector. This directly decreases the detector sensitivity. Therefore, it is crucial to maintain the alignment of the IMC to achieve the detector operation with the best performance. In order to reduce angular misalignment, an alignment sensing and control (ASC) system is adopted by using the wave front sensing (WFS) technique [5, 6].

The WFS technique is sensitive to small tilts of the mirrors, and the WFS signals are obtained by demodulating signals detected by quadrant photodiodes (QPDs) [7]. Since the signals derived by the WFSs have a Gouy phase dependence, one has to precisely estimate its behavior and choose the QPD positions carefully in order to discriminate which mirror causes misalignments in either pitch or yaw. Previous report shows the analytical calculation of the WFS signals [7, 8]. These approaches, however, contain complexities due to the fact that the non-diagonal matrix elements are fully incorporated in the calculation. Therefore, the WFS signals of the IMC have been traditionally computed by simulation tools such as Finesse [9] or Optickle [10], and it was not easy to acquire intuitive interpretations.

In this article, we present a linear approximation method

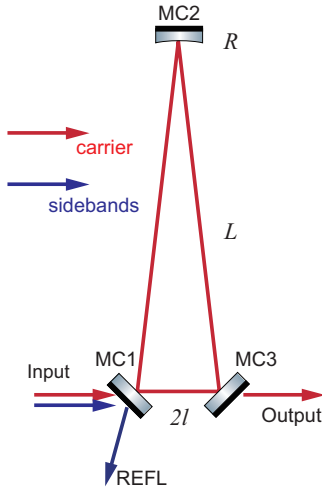


**Fig. 1.** Configuration of the IMC when the beam is injected to shorter side of the cavity. The IMC can be treated as a simple model since the carrier is on-resonant and the sidebands are off-resonant. The shorter side length  $2l$  is much smaller than longer side length  $L$ . The apex mirror (MC2) has a radius of curvature,  $R$ . The beam waist located on halfway between the two flat mirrors, MCs 1 and 3.

which enables us to relatively easily compute angular response of optical cavities. We then show the angular responses of a triangular cavity such as the shift in beam spots and the WFS signals by employing the linear approximation method. Finally, we will derive the sensing degrees of freedom (DoFs) using the singular value decomposition. Our study provides fundamental understanding with triangular optical cavities which is vital in the design and experimental phases.

## 2. A LINEAR APPROXIMATION METHOD

The  $x$  and  $y$  axes of the coordinate system are chosen to be transverse to the beam propagation ( $z$  axis) which is perfectly aligned. We additionally assume that the  $y$  axis always points upwards regardless of the propagation direction. This automatically means that the  $x$  axis needs to be mirrored every time the light is reflected by a mirror. One can expand any paraxially approximated electromagnetic fields of light beams by a set of Hermit-Gaussian (HG) modes as [11]

$$E(x, y, z) = \sum_{lm} \langle lm|E \rangle U_{lm}(x, y, z), \quad (1)$$

$$\langle lm|E \rangle \equiv \int_{-\infty}^{\infty} \int_{-\infty}^{\infty} U_{lm}^*(x, y, z) E(x, y, z) dx dy. \quad (2)$$

The coefficients  $\langle lm|E \rangle$  can be represented as the elements of the vector in the modal space. For small misalignment due to the mirror tilts, the only important modes are fundamental TEM<sub>00</sub> mode and the second lowest-order transverse modes, TEM<sub>10</sub> and TEM<sub>01</sub> [7]. Angular motions of a mirror in pitch correspond to rotations of the mirror about  $x$  axis and excites a small amount of the TEM<sub>01</sub> mode. Similarly, yaw is a rotation about the  $r$  axis, exciting a TEM<sub>10</sub> mode. For simplicity, we assume that an angular misalignment exists only in pitch and leave TEM<sub>01</sub> mode only into the consideration in the rest of this section.

We now consider a simple setup as shown in Fig. 2 and shows how the linear approximation can be placed. Although

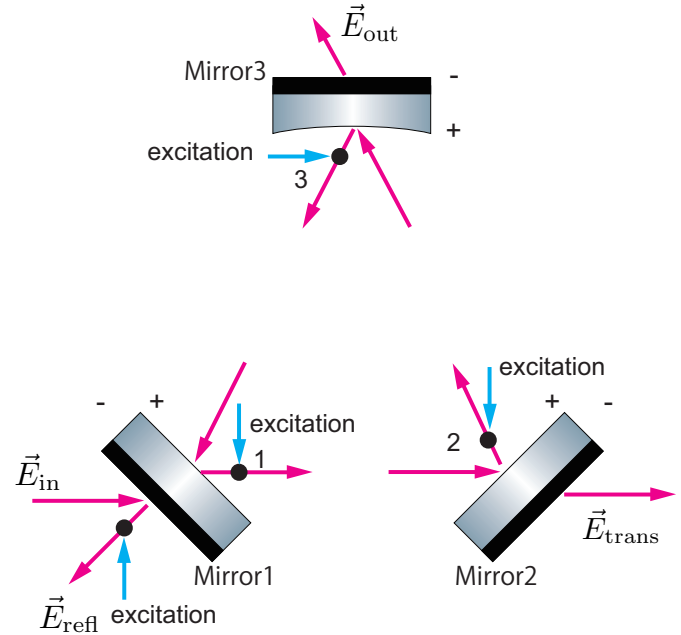


**Fig. 2.** The electric fields and nodes of a triangular cavity system. Red arrows and black dots represent electric fields and nodes, respectively. The misalignment of input mirror induces perturbation in the promptly reflection. The sign flip upon reflection of fields is labeled by "+" and "-" symbols.

a simple example is used, the argument here holds for any optical cavities as long as angular misalignment are sufficiently small. We define a collection of the field vectors containing the two sets of the fields i.e., one set from node 1 and the other from node 2.

$$\vec{E}_{00} \equiv \begin{pmatrix} \langle 00|E \rangle_1 \\ \langle 00|E \rangle_2 \\ \langle 00|E \rangle_3 \end{pmatrix}. \quad (3)$$

These fields are related to each other and can be expressed in a matrix form [12],

$$\begin{pmatrix} 0 & 0 & r_1 e^{-i\Phi_1} \\ r_2 e^{-i\Phi_2} & 0 & 0 \\ 0 & r_3 e^{-i\Phi_3} & 0 \end{pmatrix} \begin{pmatrix} \langle 00|E \rangle_1 \\ \langle 00|E \rangle_2 \\ \langle 00|E \rangle_3 \end{pmatrix} + \begin{pmatrix} t_1 \langle 00|E \rangle \\ 0 \\ 0 \end{pmatrix} = \begin{pmatrix} \langle 00|E \rangle_1 \\ \langle 00|E \rangle_2 \\ \langle 00|E \rangle_3 \end{pmatrix}, \quad (4)$$

where  $\Phi_i$  ( $i = 1, 2, 3$ ) is a one-way trip phase shift and  $r_i$  are reflectivities of each mirror. The incoming beam is assumed to be perfectly aligned to the cavity. In other words, only a TEM<sub>00</sub> mode is pumped into the system.

To reduce clutter, we introduce a matrix and vectors as

$$\hat{M}_{00} \equiv \begin{pmatrix} 0 & 0 & r_1 e^{-i\Phi_1} \\ r_2 e^{-i\Phi_2} & 0 & 0 \\ 0 & r_3 e^{-i\Phi_3} & 0 \end{pmatrix}, \quad (5)$$

$$\vec{E}_{00,\text{in}} \equiv \begin{pmatrix} t_1 \langle 00|E \rangle \\ 0 \\ 0 \end{pmatrix}. \quad (6)$$

Then, one can rewrite Eq. (4) as

$$\hat{M}_{00} \vec{E}_{00} + \vec{E}_{00,\text{in}} = \vec{E}_{00}. \quad (7)$$

Similarly, the TEM01 mode fields satisfy the following relation,

$$\hat{M}_{01} \vec{E}_{01} = \vec{E}_{01}, \quad (8)$$

where

$$\vec{E}_{01} \equiv \begin{pmatrix} \langle 01|E \rangle_1 \\ \langle 01|E \rangle_2 \\ \langle 01|E \rangle_3 \end{pmatrix}, \quad (9)$$

$$\hat{M}_{01} \equiv \begin{pmatrix} 0 & 0 & r_1 e^{-i(\Phi_1 + \eta_1)} \\ r_2 e^{-i(\Phi_2 + \eta_2)} & 0 & 0 \\ 0 & r_3 e^{-i(\Phi_3 + \eta_3)} & 0 \end{pmatrix}. \quad (10)$$

$\eta_i$  ( $i = 1, 2, 3$ ) represents a Gouy phase shift.

Small angular misalignments are introduced in pitch which transfers a fraction of the TEM00 modes to TEM01 and vice versa [7]. We will express these perturbations using normalized rotation angles,  $\Theta_i$ , ( $i = 1, 2$ ). These angles are normalized by divergence angle of the beam,  $\lambda / \pi w(z)$ , and expressed as

$$\Theta_i \equiv 2 \frac{\pi w(z)}{\lambda} \theta_i, \quad (11)$$

where the  $\theta_i$  is a small rotation of each mirror,  $\lambda$  is the wavelength of light and  $w(z)$  is a beam size at a position of  $z$  [7]. By using this normalized angle, the angular misalignment matrix is defined as

$$\hat{\Theta} \equiv \begin{pmatrix} 0 & 0 & -ir_1 e^{-i\Phi'_1} \Theta_1 \\ -ir_2 e^{-i\Phi'_2} \Theta_3 & 0 & 0 \\ 0 & -ir_3 e^{-i\Phi'_3} \Theta_2 & 0 \end{pmatrix}, \quad (12)$$

where  $\Phi'_i$  represents the one-way trip phase shift for TEM00 or TEM01 modes. Then one can express the fields with pitch angular misalignments as

$$\hat{M}_{00} \vec{E}_{00} + \vec{E}_{00,\text{in}} + \hat{\Theta} \vec{E}_{01} = \vec{E}_{00}, \quad (13)$$

$$\hat{M}_{01} \vec{E}_{01} + \hat{\Theta} \vec{E}_{00} = \vec{E}_{01}. \quad (14)$$

Since the incoming beam is pure TEM00 mode, TEM01 mode only exists when there is an angular misalignment. The fields of TEM01 mode can be written as

$$\begin{aligned} \vec{E}_{01} &= (I - \hat{M}_{01})^{-1} \hat{\Theta} \vec{E}_{00} \\ &= (I - \hat{M}_{01})^{-1} \hat{\Theta} (I - \hat{M}_{00})^{-1} (\vec{E}_{00,\text{in}} + \hat{\Theta} \vec{E}_{01}), \end{aligned} \quad (15)$$

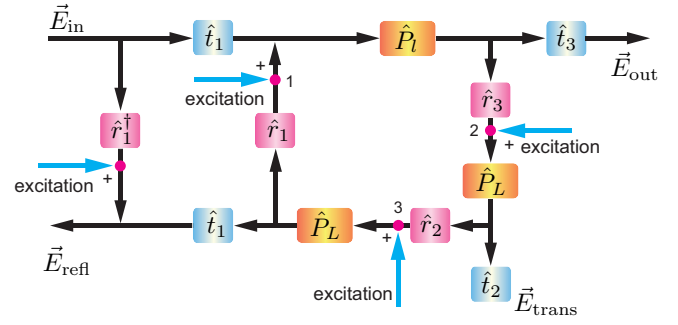


**Fig. 3.** Block diagram description of a triangular cavity with angular misalignments.  $\hat{P}$  denotes the free-space propagator between two mirrors and its subscript,  $L$  or  $l$ , correspond to the length of propagation. Each  $\hat{r}$  and  $\hat{t}$  represent reflection and transmission matrices, respectively. The labeled number, 1 to 3, denote the nodes. Angular misalignments are injected as perturbations at each node. It should be noted that promptly reflected light with MC1 angular misalignment couples to the WFS signals.

where  $I$  is the identity matrix. Here we substituted  $\vec{E}_{00}$  given by Eq. (13). Since the angular misalignment angle is so small that one can ignore higher order term  $O(\hat{\Theta}^2)$ . In fact, this is the essence of our linear approximation. With this linear approximation, TEM01 fields excited by angular misalignments can be expressed as

$$\vec{E}_{01} \approx (I - \hat{M}_{01})^{-1} \hat{\Theta} (I - \hat{M}_{00})^{-1} \vec{E}_{00,\text{in}}. \quad (16)$$

One can express TEM10 fields introduced by angular misalignments in the same manner.

Our method, in comparison to the previous study [7], obviously simplifies the resulting solutions at a cost of losing the accuracy in particular when the amount of misalignment is large. However, in practical experiments, the angular drifts are suppressed by active controls and therefore the amount of misalignment is typically small enough that our approximation is valid.

Besides, another advantage of the linearization is that the entire analysis can be expressed by a block diagram as shown in Fig. 3 similarly to those used in the classical feedback control theory [13]. Such block diagrams can help ones to acquire comprehensive physical pictures.

### 3. ANGULAR RESPONSE OF A TRIANGULAR CAVITY

We now consider the case in which a triangular cavity is in the form of isosceles triangle with the length of one side much shorter than the other two as shown in Fig. 1. The incoming laser beam is assumed to be injected to the shorter side. Fig. 3 shows a block diagram for the system with the mirrors misaligned by some small amounts.

The free-space propagator can be defined as

$$\hat{P}_{L,l} = \text{diag} \left( e^{-i\Phi_{L,l}}, e^{-i(\Phi_{L,l} - \eta_{L,l})}, e^{-i(\Phi_{L,l} - \eta_{L,l})} \right), \quad (17)$$

where its subscript,  $L$  and  $l$ , correspond to the length of propagation. The matrices  $\hat{t}$  and  $\hat{r}$  denote the transmission and reflection matrix of the mirror as,

$$\hat{r}_i = \text{diag}(r_i, -r_i, r_i), \quad (18)$$

$$\hat{t}_i = \text{diag}(t_i, t_i, t_i), \quad (19)$$

where the subscripts,  $i = 1, 2, 3$ , express each mirror of the IMC. It should be noted that the sign of reflectivity for TEM10 is negative due to the mirroring effect which flips the coordinates left-to-right in the horizontal plane. Combining these matrices, the cavity round-trip propagator,  $\hat{P}_{rt}$ , can be expressed as

$$\begin{aligned} \hat{P}_{rt} &\equiv \hat{P}_L \hat{P}_2 \hat{P}_L \hat{P}_3 \hat{P}_L \hat{P}_1 \\ &= r e^{-i\Phi_{rt}} \text{diag} \left( 1, -e^{i\eta_{rt}}, e^{i\eta_{rt}} \right), \end{aligned} \quad (20)$$

where  $r \equiv r_1 r_2 r_3$  is a total reflectivity of the system which is merely a multiplication of the amplitude reflectivity from all the mirrors and  $\eta_{rt}$  represents a round-trip Gouy phase. Using the round-trip propagator, one can express the fields inside the cavity as

$$\vec{E}_{cav} = (I - \hat{P}_{rt})^{-1} \hat{t}_1 \vec{E}_{in}. \quad (21)$$

In practical experiments, the phase modulated laser beam which can be split into the carrier and the sidebands is widely used in order to lock the laser to the cavities as shown in Fig. 1. Assuming that the cavity is kept resonant for the carrier i.e.,  $e^{-i\Phi_{rt}} = 1$ , then one can define the cavity gain for the carrier in the form of each HG modes as

$$G_{00} \equiv \frac{1}{1-r}, \quad (22)$$

$$G_{10} \equiv \frac{1}{1+re^{i\eta_{rt}}}, \quad (23)$$

$$G_{01} \equiv \frac{1}{1-re^{i\eta_{rt}}}. \quad (24)$$

It should be noted that the sign of cavity gain is flipped between TEM01 and TEM10 modes due to the mirroring effect for horizontal axis.

On the other hand, the cavity gain for the sidebands which are kept off-resonant can be written as

$$G_{00}^{SB} \equiv \frac{1}{1+r}. \quad (25)$$

Here we assumed that the reflectivity for both upper and lower sidebands are identical. When the reflectivities of mirrors are high i.e.,  $r_i \approx 1$ , the cavity gain for the sidebands are much smaller than that of the carrier. Therefore, ignoring the effect of the sidebands inside the cavity, we will consider only the carrier field for the intra-cavity fields. Then Eq. (21) can be rewritten as

$$\vec{E}_{cav} = \text{diag}(G_{00}, G_{10}, G_{01}) \hat{t}_1 \vec{E}_{in}. \quad (26)$$

Thus each HG mode excited by angular misalignment is built up inside the cavity as characterized by each cavity gain.

### A. Beam Spot Response

The response to the beam spot positions is one of the most important properties to understand the behavior of a triangular cavity. The lateral shift of the beam on each mirror can be derived by evaluating the real part of the coefficients for the 01 and 10 modes. For the purpose, let us expand a field into real and imaginary parts as,

$$A(U_{00} + CU_{01,10}) \quad (27)$$

where  $C$  is a complex number which can be expressed using a small beam translation  $a$  and a small tilt  $\alpha$  [14],

$$C = \frac{a}{w_0} + i \frac{k w_0}{2} \alpha, \quad (28)$$

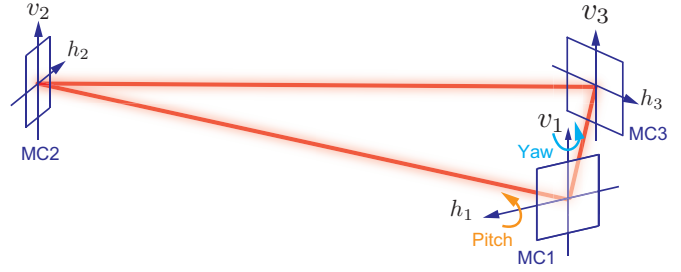


**Fig. 4.** Beam spot coordinates on mirrors and the definition of pitch and yaw rotations. Pitch and yaw are rotations around horizontal and vertical axes on a mirror, respectively.

where  $w_0$  is the beam size at its waist and  $k$  is the wavenumber. Eq. (28) tells the real part of  $C$  denotes the beam translation and the imaginary part denotes the beam tilt. Therefore, the beam spot translation can be derived from the real part of normalized coefficient,  $C$ , of TEM01/10. The notations of angular tilts and axes on the mirrors are as shown in Fig. 4.

Evaluating the real part of the field on each mirror and approximating all the mirrors to be a perfect reflector i.e.,  $r_i = 1$  ( $i = 1, 2, 3$ ), one can find the following relation between the mirror tilts and resulting variation in the beam spot as

$$\begin{pmatrix} y_1 \\ y_2 \\ y_3 \end{pmatrix} = -R \begin{pmatrix} g & 1 & g + \frac{2l}{R} \\ 1 & 1 & 1 \\ g + \frac{2l}{R} & 1 & g \end{pmatrix} \begin{pmatrix} \theta_1 \\ \theta_2 \\ \theta_3 \end{pmatrix}, \quad (29)$$

where  $g$  is the g-factor, defined as

$$g \equiv 1 - \frac{L+l}{R}, \quad (30)$$

and  $y_i$  ( $i = 1, 2, 3$ ) describe vertical displacements of the beam along the  $y$ -axis. A detailed calculation for obtaining Eq. (29) is presented in Appendix A.

Since MCs 1 and 3 have an incident angle of approximately  $\pi/4$ , the  $y_1$  axis and the  $y_3$  axis are rotated  $\pi/4$  around the  $z$  axis with respect to the  $y$  axis [9]. Therefore, an effective misalignment angle in pitch is reduced by  $\cos(\pi/4) = 1/\sqrt{2}$ , so that

$$\psi_{1,3} = \frac{1}{\sqrt{2}} \theta_{1,3}. \quad (31)$$

The axis  $y$  is same as the axis on the mirror  $v$ . Hence the beam spot displacement on the mirror can be written as

$$\begin{pmatrix} v_1 \\ v_2 \\ v_3 \end{pmatrix} = -\frac{R}{\sqrt{2}} \begin{pmatrix} g & \sqrt{2} & g + \frac{2l}{R} \\ 1 & \sqrt{2} & 1 \\ g + \frac{2l}{R} & \sqrt{2} & g \end{pmatrix} \begin{pmatrix} \psi_1 \\ \psi_2 \\ \psi_3 \end{pmatrix}. \quad (32)$$

Eq. (32) shows us how the eigenmode of triangular cavity transforms as a function of the tilt of each mirror.

Mirror positions may not always be preferable DoFs. They can be converted into the ones representing the translation and tilt of the beam at the waist, and the spot position on MC2 as

$$\begin{pmatrix} y_w \\ \theta_w \\ v_2 \end{pmatrix} \equiv \begin{pmatrix} \frac{v_1+v_3}{2} \\ \frac{v_1-v_3}{2l} \\ v_2 \end{pmatrix} = \begin{pmatrix} \frac{1}{2} & 0 & \frac{1}{2} \\ \frac{1}{2l} & 0 & -\frac{1}{2l} \\ 0 & 1 & 0 \end{pmatrix} \begin{pmatrix} v_1 \\ v_2 \\ v_3 \end{pmatrix}. \quad (33)$$

In addition, we convert the actuation basis into MCs 1 and 3 common and differential motions expressed as

$$\begin{pmatrix} \psi_c \\ \psi_d \\ \psi_2 \end{pmatrix} \equiv \begin{pmatrix} \frac{\psi_1 + \psi_3}{2} \\ \frac{\psi_1 - \psi_3}{2} \\ \psi_2 \end{pmatrix} = \begin{pmatrix} \frac{1}{2} & 0 & \frac{1}{2} \\ \frac{1}{2} & 0 & -\frac{1}{2} \\ 0 & 1 & 0 \end{pmatrix} \begin{pmatrix} \psi_1 \\ \psi_2 \\ \psi_3 \end{pmatrix}. \quad (34)$$

By using these bases, the beam spot response to pitch angular misalignment can be summarized as

$$\begin{pmatrix} y_w \\ \theta_w \\ v_2 \end{pmatrix} = \begin{pmatrix} \sqrt{2}(L-R) & 0 & -R \\ 0 & \sqrt{2} & 0 \\ -\sqrt{2}R & 0 & -R \end{pmatrix} \begin{pmatrix} \psi_c \\ \psi_d \\ \psi_2 \end{pmatrix}. \quad (35)$$

Eq. (35) shows that misalignment in MC2 cannot access to the tilt at the waist position, and only shift the plane of cavity eigenmode. Common angular tilt rotates cavity eigenmode around the center of curvature as shown in figure 19. in [15]. Differential tilt does not change the spot on the curved mirror and the waist, though the tilt at waist is rotated.

In the same way, yaw misalignment can be computed as

$$\begin{pmatrix} x_1 \\ x_2 \\ x_3 \end{pmatrix} = \begin{pmatrix} \zeta & -\frac{l}{g} & -\zeta \\ -\frac{l}{g} & \frac{L+l}{g} & -\frac{l}{g} \\ -\zeta & -\frac{l}{g} & \zeta \end{pmatrix} \begin{pmatrix} \phi_1 \\ \phi_2 \\ \phi_3 \end{pmatrix}. \quad (36)$$

where  $x_i$  is defined as  $\zeta \equiv L + l(1 - L/R)/g$ . When the displacements perpendicular to the beam,  $x_1$  and  $x_3$ , are projected on each mirror, MCs 1 and 3, the displacements on the mirror surface are enhanced by  $1/\cos(\pi/4) = \sqrt{2}$ . Therefore, Eq. (36) can be written as

$$\begin{pmatrix} h_1 \\ h_2 \\ h_3 \end{pmatrix} = \begin{pmatrix} \sqrt{2}\zeta & -\sqrt{2}\frac{l}{g} & -\sqrt{2}\zeta \\ -\frac{l}{g} & \frac{L+l}{g} & -\frac{l}{g} \\ -\sqrt{2}\zeta & -\sqrt{2}\frac{l}{g} & \sqrt{2}\zeta \end{pmatrix} \begin{pmatrix} \phi_1 \\ \phi_2 \\ \phi_3 \end{pmatrix}. \quad (37)$$

The bases can be converted in the manner same as that for pitch by using the relationship expressed as

$$\begin{pmatrix} x_w \\ \theta_w \\ h_2 \end{pmatrix} \equiv \begin{pmatrix} \frac{(h_1+h_3)\cos(\pi/4)}{2} \\ \frac{(h_1-h_3)\cos(\pi/4)}{2l} \\ h_2 \end{pmatrix} = \begin{pmatrix} \frac{1}{2\sqrt{2}} & 0 & \frac{1}{2\sqrt{2}} \\ \frac{1}{2\sqrt{2}l} & 0 & -\frac{1}{2\sqrt{2}l} \\ 0 & 1 & 0 \end{pmatrix} \begin{pmatrix} h_1 \\ h_2 \\ h_3 \end{pmatrix}, \quad (38)$$

$$\begin{pmatrix} \phi_c \\ \phi_d \\ \phi_2 \end{pmatrix} \equiv \begin{pmatrix} \frac{\phi_1 + \phi_3}{2} \\ \frac{\phi_1 - \phi_3}{2} \\ \phi_2 \end{pmatrix} = \begin{pmatrix} \frac{1}{2} & 0 & \frac{1}{2} \\ \frac{1}{2} & 0 & -\frac{1}{2} \\ 0 & 1 & 0 \end{pmatrix} \begin{pmatrix} \phi_1 \\ \phi_2 \\ \phi_3 \end{pmatrix}. \quad (39)$$

It should be noted that the effect of  $\sqrt{2}$  enhancement due to the projection on MCs 1 and 3 is cancelled. Then the beam spot response to yaw misalignments can be expressed as

$$\begin{pmatrix} x_w \\ \theta_w \\ h_2 \end{pmatrix} = \begin{pmatrix} 0 & -2L & 0 \\ \frac{2(-L+R)}{L-R+l} & 0 & -\frac{R}{L-R+l} \\ \frac{2Rl}{L-R+l} & 0 & -\frac{R(L+l)}{L-R+l} \end{pmatrix} \begin{pmatrix} \phi_c \\ \phi_d \\ \phi_2 \end{pmatrix}. \quad (40)$$

Eq. (40) shows that only misalignment in MCs 1 and 3 differential motion can access to the beam waist shift. The beam waist tilt and MC2 spot position change can be expressed by a combination of MCs 1 and 3 differential motion and MC2 motion.

These results are fully consistent with the previous analysis based on the geometrical argument [15]. Therefore, this linear approximation offers an alternative method to compute variations in the spot positions without elaborating the geometrical analysis.

## B. Wave Front Sensing Signals of the IMC

The WFS technique is sensitive to small tilts of the mirrors. The signals are obtained by demodulating the intensity information detected by quadrant photodiodes (QPDs) [7] in similar manner to the Pound-Drever-Hall (PDH) technique [16]. When one of the mirrors is misaligned, it excites the second lowest-order transverse modes, namely the TEM<sub>10</sub> or TEM<sub>01</sub> in the carrier. The WFS signals are essentially the interference between the TEM<sub>00</sub> of the sidebands and the TEM<sub>01</sub> or TEM<sub>10</sub> modes of the carrier.

We assume that the incoming light is a purely phase modulated TEM<sub>00</sub> mode described as

$$\vec{E}_{\text{in}} = \begin{pmatrix} \langle 00|E \rangle_{\text{in}} \\ 0 \\ 0 \end{pmatrix}. \quad (41)$$

Phase modulated input laser beam, which is used in PDH scheme, can be expressed as

$$\langle 00|E \rangle_{\text{in}} \approx \left[ J_0(m)e^{i\Omega t} + J_1(m)e^{i(\Omega+\omega_m)t} - J_1(m)e^{i(\Omega-\omega_m)t} \right] \times \langle 00|E \rangle \quad (42)$$

where  $\Omega$  corresponds to the angular frequency of the carrier field,  $\omega_m$  is the modulation angular frequency,  $m$  is the modulation depth and  $J_k(m)$  is Bessel functions of the first kind.

By measuring the differential of reflected field using a horizontally and vertically split photodiodes, QPD, for pitch and yaw, one can obtain the intensity information,  $S_{\text{QPD}}$ , which can be expressed as

$$S_{\text{QPD}} \propto \int_0^\infty dx \left( \vec{E}_{\text{refl}}^\dagger \cdot \vec{E}_{\text{refl}} \right) - \int_{-\infty}^0 dx \left( \vec{E}_{\text{refl}}^\dagger \cdot \vec{E}_{\text{refl}} \right). \quad (43)$$

The fields at reflection port of each mode can be calculated by multiplying propagators. The WFS signals are obtained by demodulating the signals,  $S_{\text{QPD}}$ , with the modulation angular frequency,  $\omega_m$ . After some math, one can derive the WFS signals described as

$$\text{WFS} = iP_0 J_0(m) J_1(m) \left[ U_{00}^* (G_{00} G_{10,01} e^{i\bar{\eta}} \Theta U_{10,01}) \right] \quad (44)$$

$$- U_{00} (G_{00} G_{10,01} e^{i\bar{\eta}} \Theta U_{10,01})^* \right], \quad (45)$$

where  $P_0$  denotes the optical power of the input laser beam and  $\bar{\eta}$  is a specific Gouy phase which depends on the misaligned mirror. When we apply parameters of KAGRA IMC, the WFS signals can be calculated as shown in Fig. 5.

On the other hand, aLIGO adopted a different geometry in which the laser beam is injected into the longer side of the IMC. Fig. 6 shows the WFS signals of aLIGO geometry IMC. Since MCs 1 and 3 WFS signals are highly degenerate, it is hard to distinguish between them.

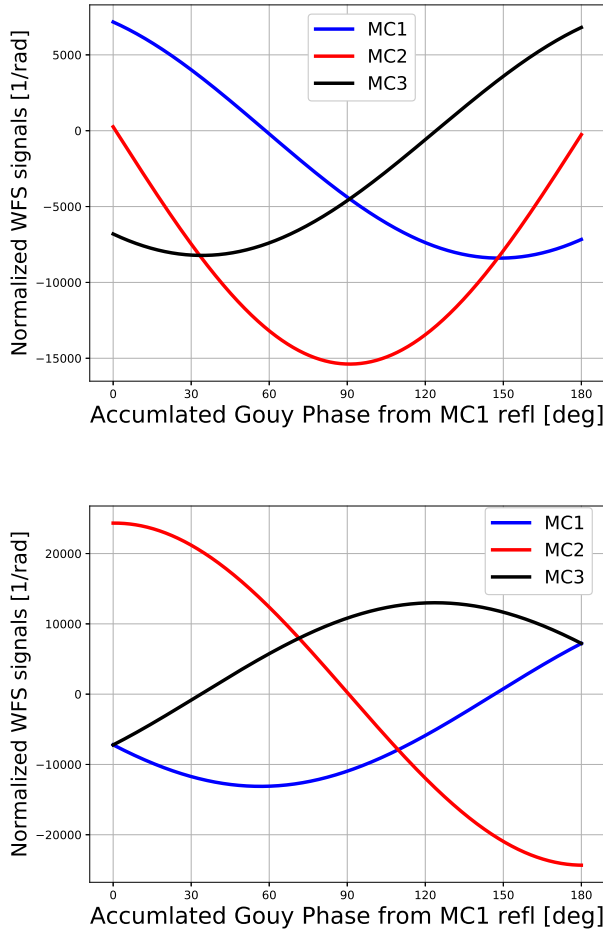


**Fig. 5.** Pitch (top) and yaw (bottom) WFS signals of shorter-side-injection geometry the IMC. We assumed that the geometrical parameters of the IMC are same as KAGRA.

#### 4. IMPLICATION TO EXPERIMENT

The IMC has three DoFs for angular misalignments in both pitch and yaw. On the other hand, the number of observable DoFs by the WFS technique is only two since the WFSs sense the difference between the two beams — the incoming and intracavity beams. In this section, the observable degrees of freedom (DoFs) of the IMC are discussed for the case where the incoming beam is injected to the shorter side of the IMC such as KAGRA [1]. For the other case where the incoming beam is injected to longer side of the IMC such as aLIGO [3], the results are shown in Appendix B for completeness.

The singular value decomposition (SVD) is one of the useful tools in order to understand what DoFs can or cannot be sensed. The SVD is widely used for data analysis [17]. The WFS signals contain beam tilt and translation components and are expressed as bellow by using a sensing matrix  $\hat{S}$ ,

$$\begin{pmatrix} \text{tilt} \\ \text{trans.} \end{pmatrix} = \hat{S} \begin{pmatrix} \theta_1 \\ \theta_2 \\ \theta_3 \end{pmatrix}, \quad (46)$$

where  $\hat{S}$  is a  $2 \times 3$  matrix and its elements can be written by us-

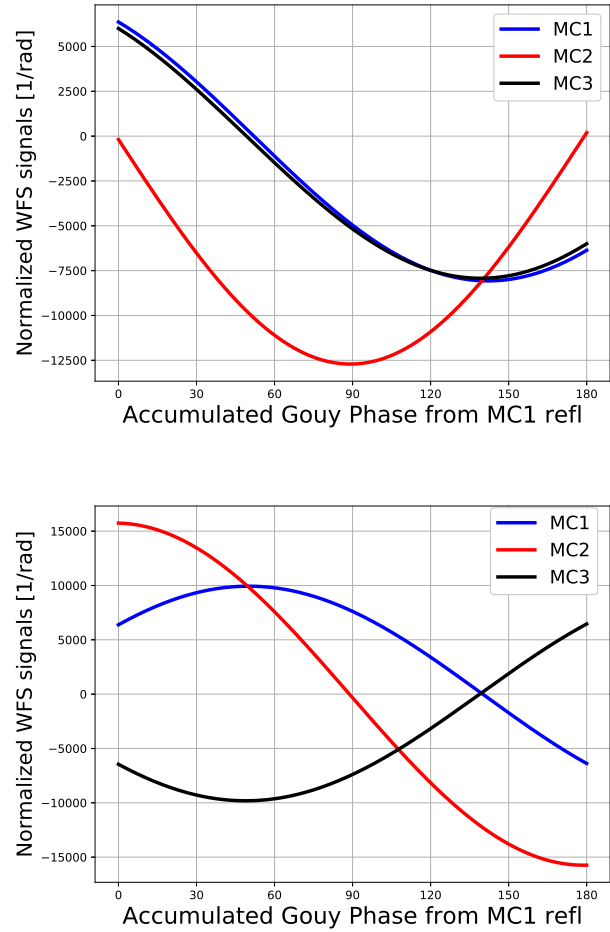


**Fig. 6.** Pitch (top) and yaw (bottom) WFS signals of longer-side-injection geometry. We assumed that the geometrical parameters of the IMC are same as aLIGO.

ing the cavity gain and Gouy phase shift. This sensing matrix can be expressed by geometrical parameters with high reflective approximation ( $r_i \approx 1$ ) and incoming beam is pure TEM00 mode. Then we will apply SVD to rewrite them to determine which DoFs are observable by the WFS technique.

In the case of the geometry used in KAGRA [1], one can obtain the relationship between the WFS signals and mirror tilt angles in pitch as

$$\begin{pmatrix} \text{tilt} \\ \text{trans.} \end{pmatrix}_{\text{Pitch}} = \sqrt{2}\gamma w_0 \begin{pmatrix} g\gamma & 0 & -g\gamma \\ -g & -\sqrt{2} & -g \end{pmatrix} \begin{pmatrix} \psi_1 \\ \psi_2 \\ \psi_3 \end{pmatrix}, \quad (47)$$

where  $\gamma \equiv (L+l)/z_R$ , and  $w_0$  is beam size at its waist. Adopting the SVD analysis, one can arrive at

$$\hat{S}_{\text{Pitch}} = \sqrt{2}\gamma w_0 I \begin{pmatrix} g\gamma & 0 & 0 \\ 0 & 1 & 0 \end{pmatrix} \begin{pmatrix} 1 & 0 & -1 \\ -g & -\sqrt{2} & -g \\ 1 & -\sqrt{2}g & 1 \end{pmatrix}. \quad (48)$$

It is clear that one the DoF shown in the lowest row in the right-most matrix. On the other hand, the first and second rows are

observable. They correspond to MCs 1 and 3 differential motion and the combination of MCs 1 and 3 common and MC2 motion, respectively. Comparing to Eq. (35), one can identify that the observable DoFs correspond to the beam waist tilt and translation.

For the case of yaw, the sensing matrix can be written as

$$\begin{pmatrix} \text{tilt} \\ \text{trans.} \end{pmatrix}_{\text{Yaw}} = \sqrt{2}\gamma w_0 \begin{pmatrix} -g & 1 & -g \\ -g\gamma & 0 & g\gamma \end{pmatrix} \begin{pmatrix} \phi_1 \\ \phi_2 \\ \phi_3 \end{pmatrix}. \quad (49)$$

The decomposed form can be expressed as

$$\hat{S}_{\text{Yaw}} = \sqrt{2}\gamma w_0 I \begin{pmatrix} g & 0 & 0 \\ 0 & g\gamma & 0 \end{pmatrix} \begin{pmatrix} -1 & \frac{1}{g} & -1 \\ -1 & 0 & 1 \\ 1 & 2g & 1 \end{pmatrix}. \quad (50)$$

The observable DoFs are the combination of MCs 1 and 3 common and MC2 motion and MCs 1 and 3 differential motion. Similarly to the pitch case, these observable DoFs correspond to the beam waist tilt and translation. Therefore, when the beam is injected to the shorter side of the IMC, the beam waist tilt and translation are observable.

## 5. CONCLUSION

We have presented the linear approximation method that can simplify the analytical calculation of angular response of optical cavities. The method enables us not only to simplify the calculation but also to make equivalent block diagrams which can bring comprehensive pictures.

The method was applied to a triangular cavity called the input mode cleaning cavity. The angular response to the shift in the beam spots and the WFS signals of the IMC in gravitational wave detectors were explicitly given by this approach. The results are consistent with the previous report which conducted a completely different approach — geometrical analysis.

Finally, the WFS sensing matrices are analyzed via the singular value decomposition scheme in order to study the observable DoFs of the IMC. When the incoming beam is injected to the shorter side of the IMC, the observable DoFs by the WFS scheme are determined to be the beam waist tilt and translation.

The linear approximation method presented in this article can be applied to optical systems which are more involved, including the main interferometer of gravitational wave detectors. The linear approximation method should be able to give deeper insight into the fundamental comprehension of the gravitational wave interferometers.

## A. CALCULATION OF BEAM SPOT MOTION

In this section, we will show one example of angular response calculation — MC3 pitch misalignment. TEM01 field at each node which is excited by MC3 pitch misalignment can be computed by multiplying propagators. The cavity gain for TEM01 can be written as

$$G_{01} = \frac{1 - \cos \eta_{rt} + i \sin \eta_{rt}}{2(1 - \cos \eta_{rt})}. \quad (51)$$

Here we introduce high reflective approximation i.e., assuming  $r \approx 1$ . In order to calculate the normalized coefficient,  $C$ , propagators must be taken into account. Then the normalized coefficient,  $C$ , at each node 1 to 3 can be written as

$$C_1 = -i\Theta_3 \frac{e^{i\eta_{MC3 \rightarrow MC1}} - e^{i(\eta_{rt} - \eta_{MC3 \rightarrow MC1})}}{2(1 - \cos \eta_{rt})} \quad (52)$$

$$C_2 = -i\Theta_3 \frac{1 - \cos \eta_{rt} + i \sin \eta_{rt}}{2(1 - \cos \eta_{rt})} \quad (53)$$

$$C_3 = -i\Theta_3 \frac{e^{i\eta_{MC3 \rightarrow MC2}} - e^{i(\eta_{rt} - \eta_{MC3 \rightarrow MC2})}}{2(1 - \cos \eta_{rt})}. \quad (54)$$

where the subscripts of Gouy phase shift such as MC3 → MC1 denote the propagation of the beam. Since the beam waist locates on halfway between MCs 1 and 3 and the length of shorter side,  $2l$ , is much smaller than that of longer side,  $L$ , Gouy phase shift can be computed as

$$\begin{aligned} \eta_{MC3 \rightarrow MC2} &= \arctan\left(\frac{L+l}{z_R}\right) - \arctan\left(\frac{l}{z_R}\right) \\ &\approx \arctan\left(\frac{L+l}{z_R}\right), \end{aligned} \quad (55)$$

where  $z_R$  represents the Rayleigh length expressed as

$$z_R = \sqrt{(L+l)(R-L-l)}. \quad (56)$$

Due to the apex mirror with radius of curvature, the Gouy phase shift from MC3 to MC1 becomes  $\eta_{MC3 \rightarrow MC1} = 2 \times \eta_{MC3 \rightarrow MC2}$ . By using the relationships between the beam size at waist and Rayleigh length expressed as

$$w_0 = \sqrt{\frac{z_R \lambda}{\pi}}, \quad (57)$$

and the trigonometric functions and inverse trigonometric functions described as

$$\sin(\arctan(x)) = \frac{x}{\sqrt{1+x^2}}, \quad (58)$$

we can calculate the real part of each normalized coefficient as

$$\mathcal{R}\{C_1\} = R \left( g + \frac{2l}{R} \right) \theta_3, \quad (59)$$

$$\mathcal{R}\{C_2\} = Rg\theta_3, \quad (60)$$

$$\mathcal{R}\{C_3\} = R\theta_3. \quad (61)$$

One can compute other beam spot response as the same manner. Hence, the beam shift on each mirror surface due to MC3 pitch misalignment can be described as Eqs. (29) and (36).

## B. OBSERVABLE DOFS OF ALIGO IMC

We will consider the observable DoFs of the IMC when the beam is injected to the longer side of the IMC such as aLIGO [3]. In this case, the WFS signals in pitch can be expressed as

$$\begin{pmatrix} \text{tilt} \\ \text{trans.} \end{pmatrix}_{\text{Pitch}} = \sqrt{2}\gamma w_0 \begin{pmatrix} g\gamma & 0 & g\gamma \\ -g & -\sqrt{2} & -g \end{pmatrix} \begin{pmatrix} \psi_1 \\ \psi_2 \\ \psi_3 \end{pmatrix}. \quad (62)$$

This sensing matrix can be decomposed by SVD as the same manner as short-side-injection case. The decomposed sensing matrix of pitch can be written as

$$\hat{S}_{\text{Pitch}} = I \begin{pmatrix} \sigma_1 & 0 & 0 \\ 0 & \sigma_2 & 0 \end{pmatrix} \begin{pmatrix} 1 & a & -1 \\ -g & b & -g \\ 1 & 0 & -1 \end{pmatrix}, \quad (63)$$

where  $\sigma_{1,2}$  are singular values of sensing matrix. Here we used  $a$  and  $b$  since these elements are In the case of aLIGO IMC, the SVD form sensing matrix is more complicated than the case of KAGRA-like configuration and the observable DoFs are difficult to interpret. On the other hand, one can discriminate the DoF we cannot sense corresponds to the beam waist tilt.

In order to know the observable DoFs, the unitary rotation matrix is adopted,  $R(\theta)$ , which satisfy following relation

$$R(\theta)_{\text{Pitch}} \begin{pmatrix} 1 & a & -1 \\ -g & b & -g \\ 1 & 0 & -1 \end{pmatrix} = \begin{pmatrix} \text{trans.} \\ \text{MC2} \\ \text{tilt} \end{pmatrix}. \quad (64)$$

By introducing this rotation matrix to Eq. (63), the decomposed sensing matrix can be expressed as

$$\hat{S}_{\text{Pitch}} = I \begin{pmatrix} \sigma_1 & 0 & 0 \\ 0 & \sigma_2 & 0 \end{pmatrix} R^T(\theta)_{\text{Pitch}} \begin{pmatrix} \text{trans.} \\ \text{MC2} \\ \text{tilt} \end{pmatrix}. \quad (65)$$

One can see that we can sense the beam waist translation and MC2 spot position by the WFS.

As the same manner as pitch case, for the case of yaw, we can obtain the SVD form sensing matrix with rotation matrix as

$$\hat{S}_{\text{Yaw}} = I \begin{pmatrix} \sigma_1 & 0 & 0 \\ 0 & \sigma_2 & 0 \end{pmatrix} \begin{pmatrix} 1 & a_{\text{Yaw}} & -1 \\ -g & b_{\text{Yaw}} & -g \\ 1 & 0 & -1 \end{pmatrix}, \quad (66)$$

Similarly to the case of pitch, we can define the unitary rotation matrix such that

$$R(\theta)_{\text{Yaw}} \begin{pmatrix} 1 & a' & -1 \\ -g & b' & -g \\ 1 & 0 & -1 \end{pmatrix} = \begin{pmatrix} \text{trans.} \\ \text{MC2} \\ \text{tilt} \end{pmatrix}. \quad (67)$$

Therefore, the sensing matrix for yaw can be decomposed as

$$\hat{S}_{\text{long,Yaw}} = I \begin{pmatrix} \sigma_1 & 0 & 0 \\ 0 & \sigma_2 & 0 \end{pmatrix} R^T(\theta)_{\text{Yaw}} \begin{pmatrix} \text{trans.} \\ \text{MC2} \\ \text{tilt} \end{pmatrix}. \quad (68)$$

Thus, the observable DoFs are consisted by beam waist translation and MC2 beam spot motion. Since the IMC has much smaller short side than longer side, the observable composed by beam waist translation and MC2 beam spot can be approximately regarded as the motion of longer side axis of the IMC. Therefore, one possible interpretation of observable of aLIGO IMC is the shift of longer side axis.

## FUNDING

This work was supported by MEXT, JSPS Leading-edge Research Infrastructure Program, JSPS Grant-in-Aid for Specially Promoted Research 26000005, JSPS Grant-in-Aid for Scientific Research on Innovative Areas 2905: JP17H06358, JP17H06361 and JP17H06364, JSPS Core-to-Core Program A. Advanced Research Networks, JSPS Grant-in-Aid for Scientific Research (S) 17H06133, the joint research program of the Institute for Cosmic Ray Research, University of Tokyo, National Research Foundation (NRF) and Computing Infrastructure Project of KISTI-GSDC in Korea, Academia Sinica (AS), AS Grid Center (ASGC) and the Ministry of Science and Technology (MoST) in Taiwan under grants including AS-CDA-105-M06, the LIGO project, and the Virgo project.

## ACKNOWLEDGEMENTS

This paper has JGW Document No. JGW-P2011199.

## DISCLOSURE

The authors declare no conflicts of interest.

## REFERENCES

1. Y. Aso, Y. Michimura, K. Somiya, M. Ando, O. Miyakawa, T. Sekiguchi, D. Tatsumi, and H. Yamamoto, "Interferometer design of the kagra gravitational wave detector," *Phys. Rev. D* **88**, 043007 (2013).
2. I. Ushijima, M. Takamoto, and H. Katori, "Operational Magic Intensity for Sr Optical Lattice Clocks," *Phys. Rev. Lett.* **121**, 263202 (2018).
3. C. L. Mueller, M. A. Arain, G. Ciani, R. T. DeRosa, A. Effler, D. Feldbaum, V. V. Frolov, P. Fulda, J. Gleason, M. Heintze, K. Kawabe, E. J. King, K. Kokeyama, W. Z. Korth, R. M. Martin, A. Mullavey, J. Peold, V. Quetschke, D. H. Reitze, D. B. Tanner, C. Vorvick, L. F. Williams, and G. Mueller, "The advanced LIGO input optics," *Rev. Sci. Instruments* **87**, 014502 (2016).
4. S. Nagano, M. A. Barton, H. Ishizuka, K. Kuroda, S. Matsumura, O. Miyakawa, S. Miyoki, D. Tatsumi, T. Tomaru, T. Uchiyama, M. Ando, K. Arai, K. Kawabe, N. Ohishi, A. Takamori, S. Taniguchi, K. Tochikubo, K. Tsubono, K. Yamamoto, M.-K. Fujimoto, M. Fukushima, S. Kawamura, Y. Kozai, S. Miyama, M. Ohashi, S. Sato, R. Takahashi, S. Telada, T. Yamazaki, N. Mio, S. Moriwaki, G. Horikoshi, N. Kamikubota, Y. Ogawa, Y. Saito, T. Suzuki, M. Musha, K. Nakagawa, A. Ueda, K.-i. Ueda, A. Araya, N. Kanda, T. Nakamura, T. Tanaka, M. Sasaki, H. Tagoshi, T. Futamase, N. Kawashima, E. Mizuno, Y. Kojima, N. Matsuda, K.-i. Oohara, and N. Tsuda, "Development of a light source with an injection-locked Nd:YAG laser and a ring-mode cleaner for the TAMA 300 gravitational-wave detector," *Rev. Sci. Instruments* **73**, 2136–2142 (2002).
5. E. Morrison, B. J. Meers, D. I. Robertson, and H. Ward, "Automatic alignment of optical interferometers," *Appl. Opt.* **33**, 5041–5049 (1994).
6. N. Mavalvala, D. Sigg, and D. Shoemaker, "Experimental test of an alignment-sensing scheme for a gravitational-wave interferometer," *Appl. Opt.* **37**, 7743–7746 (1998).
7. Y. Hefetz, N. Mavalvala, and D. Sigg, "Principles of calculating alignment signals in complex resonant optical interferometers," *J. Opt. Soc. Am. B* **14**, 1597–1606 (1997).
8. D. Sigg and N. Mavalvala, "Principles of calculating the dynamical response of misaligned complex resonant optical interferometers," *J. Opt. Soc. Am. A* **17**, 1642–1649 (2000).
9. A. Freise, D. Brown, and C. Bond, "Finesse, Frequency domain INterferometer Simulation Software," (2013).
10. M. Evans, "Optickle LIGO Document T070260-00," <https://dcc.ligo.org/public/0027/T070260/001/Optickle.pdf>.
11. A. E. Siegman, *Lasers* (University Science Books, 1986).



12. A. Freise and K. Strain, "Interferometer techniques for gravitational-wave detection," *Living Rev. Relativ.* **13**, 1 (2010).
13. B. Lurie and P. Enright, *Classical Feedback Control: With MATLAB*, Automation and Control Engineering (Taylor & Francis, 2000).
14. K. Kawabe, N. Mio, and K. Tsubono, "Automatic alignment-control system for a suspended Fabry–Perot cavity," *Appl. Opt.* **33**, 5498–5505 (1994).
15. F. Kawazoe, R. Schilling, and H. Lück, "Eigenmode changes in a misaligned triangular optical cavity," *J. Opt.* **13**, 055504 (2011).
16. R. W. P. Drever, J. L. Hall, F. V. Kowalski, J. Hough, G. M. Ford, A. J. Munley, and H. Ward, "Laser phase and frequency stabilization using an optical resonator," *Appl. Phys. B* **31**, 97–105 (1983).
17. O. Alter, P. O. Brown, and D. Botstein, "Singular value decomposition for genome-wide expression data processing and modeling," *Proc. Natl. Acad. Sci.* **97**, 10101–10106 (2000).